Automatic Subcortical Structure Segmentation using Local Likelihood-based Active Contour

Jundong Liu[1], Charles Smith[2], Hima Chebrolu[2]

[1]School of Electrical Engineering & Computer Science
Ohio University
Athens, OH
[2]Department of Neurology
University of Kentucky
Lexington, KY

Abstract. In this paper, we propose a local likelihood-based active contour model for subcortical structure segmentation. As a generalization of the Chan-Vese piecewise-constant model, our solution uses Bayesian *a posterior* probabilities as the driving forces for curve evolution. Distribution prior for the structure of interest, e.g., caudate nucleus, can be seamlessly integrated into the level set evolution procedure, and no thresholding step is needed for capturing the target. Unlike other region-based active contour models, our solution relaxes the global piecewise-constant assumption, and uses locally varying Gaussians to better account for intensity inhomogeneity and local variations existing in many MR images. More accurate and robust segmentations are therefore achieved.

1 Introduction

Magnetic resonance imaging (MRI) is a rich source of information regarding the soft tissue anatomy of human brains. Segmentation of the whole brain as well as the subcortical structures from MR image is a critical and fundamental task for the large volume of 3D MRI data to be effectively utilized for disease diagnosis, functional analysis of brains and the treatment of disease related to brain anomalies.

A variety of approaches to brain MRI segmentation have been proposed in the literature. Regional-based active contour models [1, 11, 3] have gained great attention and popularity in recent years. Active contour without edge model, commonly known as the Chan-Vese piecewise-constant model [1], uses a stopping term based on the Mumford-Shah segmentation functional so that the model can detect object boundaries with or without gradient. These methods, however, when applied to segmenting subcortical structures, usually require certain user interaction in curve initialization and/or segmentation post-processing.

Many popular subcortical structure segmentation algorithms [12, 8, 10, 11, 6] involve combining certain registration technique with an atlas. The final segmentation is obtained by aligning the previously segmented template with the

T. Heimann, M. Styner, B. van Ginneken (Eds.): 3D Segmentation in The Clinic:
A Grand Challenge, pp. 91-98, 2007.

subject. Atlases, either probabilistic distribution-based [12, 10, 8] or shape-based [11, 6], play a crucial role in securing the robustness and accuracy of the segmentation results.

This paper describes a fully automatic subcortical structure segmentation solution that utilizes a distribution atlas built from a set of training MR images. It is a straightforward extension of our previously published **Local Gaussian-based Active Contour (LGAC)** model for whole brain segmentation (accepted for oral presentation in BMVC'07). The LGAC model is formulated under Bayesian a posterior probability framework, and it differs from other major region-based active contour models in two aspects: 1) distribution prior can be seamlessly integrated into the level set evolution procedure and leads to more robust segmentations; 2) piecewise constant assumption is relaxed from "global" to "local", and *local means* are used as the area representatives. Being able to better account for intensity inhomogeneity, our LGAC model works particularly well for the images with low intensity contrasts and spatially varying brightness variations. The extension made in this paper is to apply this model to caudate segmentation.

2 Local Gaussian-based Active Contour (LGAC) Model

Let C be an evolving curve in Ω. C_{in} denotes the region enclosed by C and C_{out} denotes the region outside of C. Let $S = \{in, out\}$ be the two classes for a two-phase model. The probability of the pixel (x, y) belonging to in and out is denoted by $P(in|(x, y))$ and $P(out|(x, y))$ respectively. Let $Pr(in)$ and $Pr(out)$ be the class prior probabilities at (x, y). Then,

$$P(in|u_0(x,y)) = \frac{Pr(in_{(x,y)})P(u_0(x,y)|in)}{P(B)}$$
$$P(out|u_0(x,y)) = \frac{Pr(out_{(x,y)})P(u_0(x,y)|out)}{P(B)}$$

where $P(u_0(x, y)|in)$ is the likelihood of a voxel in class in has the intensity of $u_0(x, y)$. $P(B)$ is a constant. The maximum a posterior segmentation would be achieved only if the multiplication of $P(in|(x, y))$ and $P(out|(x, y))$ all over the entire image domain is maximized. Taking a logarithm, the maximization can be reduced to the minimization of the following energy:

$$F(C) = \mu \cdot \text{Length}(C) - \int_{C_{in}} \log(Pr(in)P(u_0(x,y)|in))dxdy$$
$$- \int_{C_{out}} \log(Pr(out)P(u_0(x,y)|in))dxdy$$

Spatial distribution priors – Caudate atlas: Two sets of training data for Caudate segmentation have been provided by the organizers of the MICCAI Workshop on 3D Segmentation in the Clinic. One set is part of the internet

brain segmentation repository (IBSR) at Mass General Hospital, and the other from the Psychiatry Neuroimaging Laboratory at the Brigham and Womens Hospital Boston. In this paper, we picked the second data set (BWH_PNL) for building the probabilistic atlas. The experiments conducted were also focused onto BWH_PNL testing data only.

The template brain provided by SPM2 [9], obtained based on 152 brains from Montreal Neurological Institute, has been used as the standard space. BWH_PNL training set contains 15 images. Each of them, $f_i (1 \leq i \leq N = 15)$ has a corresponding segmentation $s_i (1 \leq i \leq N)$ for the caudate structure. Let r denote the standard template. The probabilistic caudate atlas was constructed as follows

1. For each training image f_i in the BWH_PNL data sets, normalize it to the standard template r using SPM2's normalization routine. A 12-parameters affine transformation is estimated first, followed by a nonlinear warping based on a linear combination of discrete cosine transform (DCT) basis functions. The resulting transformation is denoted as T_i.
2. Apply T_i to s_i to get a transformed caudate segmentation s_i'.
3. Sum up s_i' under the standard space to get ss'.
4. The prior distribution is then obtained: $Pr(Caudate) = \frac{ss'}{N}$, and $Pr(NonCaudate) = 1 - P(Caudate)$.

When we try to segment the caudate of a testing image k, an affine transformation from the standard template r to k is estimated using SPM2. Then the obtained transformation is applied to the distribution atlas $Pr'(Caudate)$ and $Pr'(NonCaudate)$ to put the prior images on the aligned space with the testing image k.

Likelihood terms $P(u_0(x,y)|in)$ and $P(u_0(x,y)|out)$: global Gaussians are commonly assumed in many region-based active contour models to model the intensity distribution, but they are often not an accurate description of the local image profile, especially when intensity inhomogeneity is present. A remedy is to relax the global Gaussian mixture assumption and take local intensity variations into consideration. More specifically, local Gaussians (local binary is the degenerate case) should be used as a better approximation to model the vicinity of each voxel.

In the Chan-Vese model, two global means c_1 and c_2 are computed for C_{in} and C_{out}. In our approach, we introduce two functions $v_1(x,y)$ and $v_2(x,y)$, both defined on the image domain, to represent the mean values of the *local* pixels inside and outside the moving curve. By *Local*, we mean that only neighboring pixels will be considered. A simple implementation of the "neighborhood" is to introduce a rectangular window $W(x,y)$ with size of $2k+1$ by $2k+1$, where k is a constant integer. Therefore,

$$v_1(x,y) = \text{mean}(u_0 \in (C_{in} \cap W(x,y)))$$
$$v_2(x,y) = \text{mean}(u_0 \in (C_{out} \cap W(x,y)))$$

With the new setup, our segmentation model can then be updated as a minimization of the following energy:

$$F(v_1, v_2, C) = \mu \cdot \text{Length}(C) - \int_{C_{in}} \left(\log(Pr(in)) - \log(\sigma_1) - \frac{(u_0 - v_1)^2}{2\sigma_1^2} \right) dxdy - \int_{C_{out}} \left(\log(Pr(out)) - \log(\sigma_2) - \frac{(u_0 - v_2)^2}{2\sigma_2^2} \right) dxdy \quad (1)$$

where *in* in this paper represents the class of *Caudate* and *out* for *NonCaudate*.

2.1 Level set framework and gradient flow

Using the Heavside function H and the one-dimensional Dirac measure δ [1], the energy function $F(v_1, v_2, C)$ can be minimized under the level set framework, where the update will be conducted on the level set function ϕ. Parameterizing the descent direction by an artificial time $t \geq 0$, the gradient flow for $\phi(t, x, y)$ is given from the associated Euler-Lagrange equation as

$$\frac{\partial \phi}{\partial t} = \text{sign}(v_1 - v2) \cdot \delta(\phi) \left[\mu \text{div}(\frac{\nabla \phi}{|\nabla \phi|}) - \log \frac{Pr'(Caudate)}{Pr'(NonCaudate)} + \log \frac{\sigma_1}{\sigma_2} - \left(\frac{(u_0 - v_1)^2}{2\sigma_1^2} - \frac{(u_0 - v_2)^2}{2\sigma_2^2} \right) \right] \quad (2)$$

where ϕ_0 is the level set function of the initial contour. This gradient flow is the evolution equation of the level set function of our proposed method.

Correspondingly, v_1 and v_2 are computed with

$$v_1 = \frac{(u_0 * H(\phi)) \otimes W}{H(\phi) \otimes W} \qquad v_2 = \frac{(u_0 * (1 - H(\phi))) \otimes W}{(1 - H(\phi)) \otimes W} \quad (3)$$

where $\otimes$ is the convolution operator. One should note that, Chan-Vese model can be regarded as a special case of our model — when the window W is set to infinitely large.

The sign(v_1 - v_2) term in Eqn.2 is designed to avoid the occurrence of an undesired curve evolution phenomenon we named as *local twist*. When *Local twist* happens, the multiple components of a same class might be evolved into the opposite side of ϕ, therefore labeled with different classes. sign(v_1 - v_2) is a simple yet effective way to prevent this phenomenon from happening. More details can be found in our BMVC paper [7].

In practice, the Heaviside function H and Dirac function δ in eqn. 2 have to be approximated by smoothed versions. We adopt the $H_{2,\epsilon}$ and $\delta_{2,\epsilon}$ used in [1]. For all the experiments conducted in this paper, we set the size of the window W as 21×21.

3 Results and Discussions

We applied our method to the 14 BWH testing data sets. Fig 1 shows the segmentation result on a subject in the adults BWH group. The reference standard segmentation and our segmentation are outlined in red and blue, respectively. In our implementation, the GM/WM two-phase level set function was initialized based on the a thresholding of the probability map. We chose 0.2 as the threshold in all experiments, but any values from 0.1 to 0.5 would generate similar segmentation results. The curvature term constant μ in Eqn. (2) is set to 1 in the experiments. Increasing the value of μ or adding frequent level set re-initialization would enhance the smoothness and regularity of the level set function, therefore potentially improve the segmentation quality of our model.

We also tested our LGAC model on the UNC data sets, but it seemed that our model couldn't separate the gray matter (both cortical and sub-cortical) from the white matter.

Fig 2 gives the results of the comparison metrics and corresponding scores for all test cases averaged for the left and right segmentation. Out of the 14 test data sets, our algorithm failed twice (BWH_PNL 22 and BWH_PNL 26). In additional to the overall average across the all test cases, the statistics for "successful cases only" are also listed at the end the table. Fig 3 shows Pearson correlation for the volume measurements in the BWH testing group.

Program running time: the algorithm presented in this paper is implemented with Matlab 7 R14, under an IBM Thinkpad T60 laptop (Intel Core Duo T2300 / 1.66 GHz processor, 2.0GB of RAM). The average running time for BWH data is around 15 minutes per set. The level set update routine is implemented purely using Matlab m-files so far. We expect a significant reduce in the whole running time after the core level set part is implemented with mex-C.

References

1. T. F. Chan and L. A. Vese, "Active contours without edges", IEEE Trans. on Image Processing, Vol. 10, No. 2, pp. 266-277, 2001.
2. C. A. Cocosco et al., "BrainWeb: Online interface to a 3D MRI simulated brain database", Neuroimage, Vol. 5, No. 4, S245, 1997.
3. D. Cremers, M. Rousson and R. Deriche, "A review of statistical approaches to level set segmentation: integrating color, texture, motion and shape", IJCV, Vol. 72, No. 2, pp. 195-215, 2007.
4. J. Yang, H. Tagare, L. H. Staib, J. S. Duncan, "Segmentation of 3D Deformable Objects with Level Set Based Prior Models". ISBI'04, pp. 85-88, 2004.
5. A. C. Evans, D. L. Collins and B. Milner, "An MRI-based stereotactic atlas from 250 young normal subjects", Society of Neuroscience Abstrasts, 18:408, 1992.
6. M. Leventon, W. Grimson, and O. Faugeras, "Statistical shape influence in geodesic active contours" CVPR'00, Vol. 1, pp. 316-323, 2000.
7. J. Liu, D. Chelberg, C. Smith and H. Chebrolu, "A Likelihood-based Active Contour Model for Medical Image Segmentation.", to appear in British Machine Vision Conference (BMVC'07), 10-13 September, Warwick, UK, 2007.

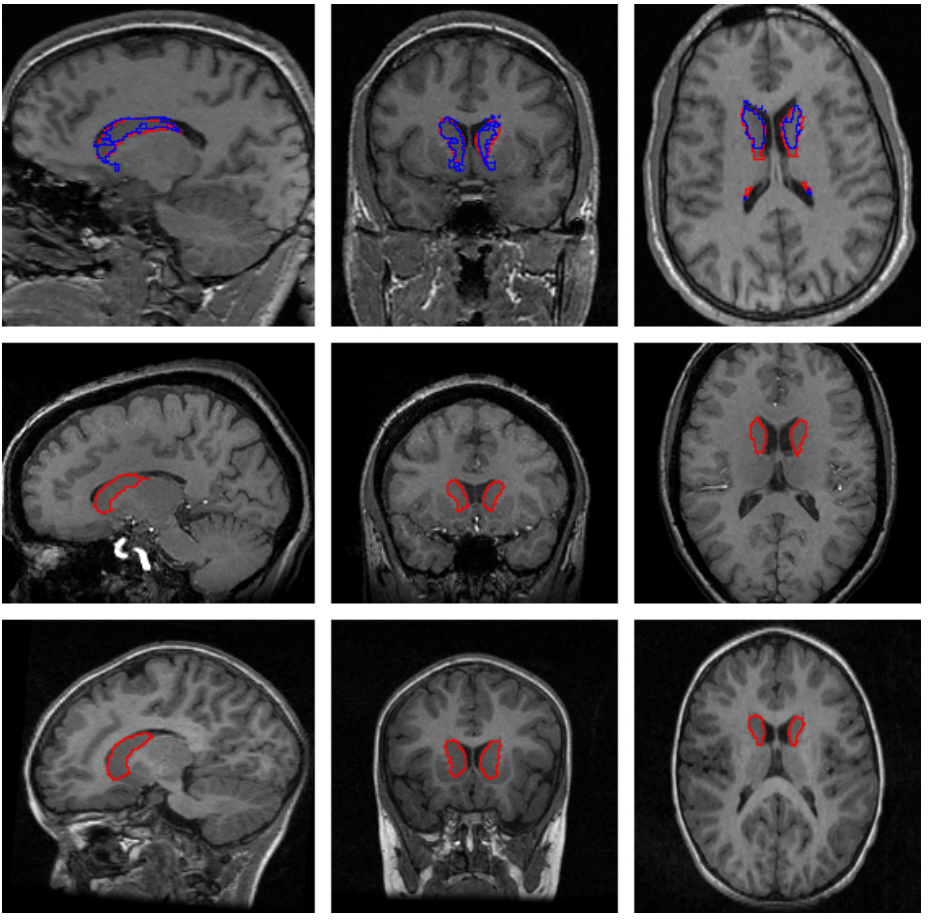

Fig. 1. From left to right, a sagittal, coronal and transversal slice from a a subject in the adults BWH group. The outline of the reference standard segmentation is in red, the outline of the segmentation of the method described in this paper is in blue.

8. K. Pohl, S. Bouix, R. Kikinis, and W. Grimson, "Anatomical guided segmentation with non-stationary tissue class distributions in an expectation-maximization framework,", ISBI'04, pp. 81-84, 2004.
9. A. Mechelli, C.J. Price, K.J. Friston, and J. Ashburner. "Voxel-Based Morphometry of the Human Brain: Methods and Applications". Current Medical Imaging Reviews, pp. 105-113, 2005.
10. S. Gouttard, M. Styner, S. Joshi, and G. Gerig, "Subcortical structure segmentation using probabilistic atlas prior", Proc SPIE Medical Imaging Conference, Vol 6512, pp. 65122J-1-65122J-11, 2007.
11. A. Tsai, A. Yezzi, W. Wells, C. Tempany, D. "Approach to Curve: Evolution for Segmentation of Medical Imagery", IEEE TMI, Vol. 22, No. 2, pp. 137-154, February 2003.

All Dataset	Overlap Err		Volume Diff.		Abs. Dist.		RMS Dist.		Max. Dist.		Total
	[%]	Score	[%]	Score	[mm]	Score	[mm]	Score	[mm]	Score	Score
UNC Ped 10	100.0	0	100.0	0	30.0	0	30.0	0	30.0	0	0
UNC Ped 14	100.0	0	100.0	0	30.0	0	30.0	0	30.0	0	0
UNC Ped 15	100.0	0	100.0	0	30.0	0	30.0	0	30.0	0	0
UNC Ped 19	100.0	0	100.0	0	30.0	0	30.0	0	30.0	0	0
UNC Ped 30	100.0	0	100.0	0	30.0	0	30.0	0	30.0	0	0
UNC Eld 01	100.0	0	100.0	0	30.0	0	30.0	0	30.0	0	0
UNC Eld 12	100.0	0	100.0	0	30.0	0	30.0	0	30.0	0	0
UNC Eld 13	100.0	0	100.0	0	30.0	0	30.0	0	30.0	0	0
UNC Eld 20	100.0	0	100.0	0	30.0	0	30.0	0	30.0	0	0
UNC Eld 26	100.0	0	100.0	0	30.0	0	30.0	0	30.0	0	0
BWH PNL 16	41.9	74	9.2	84	0.8	70	1.4	74	8.6	75	76
BWH PNL 17	37.9	76	-5.2	91	0.8	70	1.7	69	14.9	56	73
BWH PNL 18	39.1	76	-21.0	63	1.1	60	2.4	58	19.9	42	60
BWH PNL 19	44.9	72	-4.1	90	1.1	60	2.1	62	15.7	54	68
BWH PNL 20	37.0	77	7.2	77	0.7	74	1.7	70	16.8	50	70
BWH PNL 21	57.1	64	-36.2	36	1.3	50	2.2	60	13.0	62	54
BWH PNL 22	88.3	44	17.2	70	8.9	0	11.5	0	26.6	22	27
BWH PNL 23	34.0	79	14.6	74	0.7	72	1.5	74	8.4	75	75
BWH PNL 24	37.3	76	9.3	84	0.9	66	1.9	66	15.9	54	69
BWH PNL 25	47.2	70	-8.5	84	1.5	44	3.5	38	28.7	16	50
BWH PNL 26	51.3	68	20.8	64	2.0	26	4.2	25	25.1	26	42
BWH PNL 27	36.4	77	-11.1	80	0.9	68	1.9	66	15.3	55	69
BWH PNL 28	49.9	68	-16.4	71	1.1	60	2.1	62	15.5	54	63
BWH PNL 29	36.4	77	18.7	67	0.8	70	1.9	66	13.9	59	68
Average All	68.3	42	41.4	43	13.4	33	14.2	33	22.4	29	36
Average UNC Ped	100.0	0	100.0	0	30.0	0	30.0	0	30.0	0	0
Average UNC Eld	100.0	0	100.0	0	30.0	0	30.0	0	30.0	0	0
Average BWH PNL	45.6	71	-0.4	74	1.6	56	2.9	56	17.0	50	62

Fig. 2. Results of the comparison metrics and corresponding scores for all test cases averaged for the left and right segmentation. The summary rows at the end of the table display the overall average across all test cases, as well as grouped for the three testing groups. The algorithm failed for two cases, BWH_PNL 22 and BWH_PNL 26.

Correl	UNC Ped	UNC Eld	BWH PNL	Total
Left	nan	nan	-0.0103	nan
Right	nan	nan	0.2022	nan
Average	nan	nan	0.0960	nan

Fig. 3. Pearson correlation for the volume measurements in the three testing groups as well as in total. This coefficient captures how well the volumetric measurements correlate with those of the reference segmentations.

12. J. Zhou and J. C. Rajapakse, "Segmentation of subcortical brain structures using fuzzy templates", NeuroImage, Vol. 28, No. 4, pp. 915-924, December 2005.